Research Article

# Finite element simulation of X20CrMoV121 steel billet forging process using the Deform 3D software

J. O. Obiko[1,2] · F. M. Mwema[3,4] · M. O. Bodunrin[1,5]



**Abstract**
In this article, a three-dimensional finite element analysis using Deform 3D software has been employed to investigate the plastic deformation behavior during forging of X20CrMoV121 steel. The focus was on the influence of forging temperature on the strain, stress and particle flow velocity distribution during the forging process. From the results, it has been shown that the forging process results in inhomogeneous plastic deformation, hence inhomogeneous strain, stress, and particle flow velocity distribution. As the temperature increased from 800 to 1100 °C, the forging loads and the deformation resistance were observed to decrease with an increase. For each temperature, the load increased rapidly with the stroke and then the increase slowed. This behavior was related to the coefficient of friction at the tool sample interface. It was also shown that the maximum effective stress/strain decreased as the forging temperature increased to 1100 °C. It is suggested that 3D finite element simulation by Deform® 3D software is an efficient method for predicting metal flow behavior during the forging process.

**Keyword** Finite element analysis · Forging · Plastic deformation · Forging load · Metal flow

## 1 Introduction

In metal working processes, plastic deformation is used to alter the shape and improve the properties of metallic specimens. Some of the most common industrial metal forming processes include rolling, forging, extrusion and drawing [1, 2]. During these production process, metallic materials are subjected to large plastic deformation [3]. For example, forging (upsetting) process involves large deformation forces and stresses and therefore the material flow in deformation analysis is very complex [4], since the flow stress and strain distribution depend on the deformation temperature, strain rate and strain [5]. Physical simulation processes such as the Gleeble® thermal mechanical simulators have been widely applied to predict and simulate the industrial metalworking processes [5–9]. However, these laboratory processes encounter optimization challenges associated with the deformation process such as the evolution of heat due to the frictional forces between the anvil and workpiece [10], thus affecting the flow behavior. The generation of heat makes the production process complex and inhomogeneous and therefore affecting the properties of product [11]. Traditionally, the industrial production process depends on the experience of the designer and trial and error method, hence a costly process [ [1], [12] ]. As such, process optimization is necessary to reduce the production cost by using a more efficient approach to design metal forming processes [12]. Recently, finite element modeling (FEM) computer software programs such as Deform® 3D, AbaQus, Marc, ANSYS, etc. have been used to evaluate and optimize the most common metal forming processes [13, 14], leading to the reduction of

✉ F. M. Mwema, fredrick.mwema@dkut.ac.ke | [1]School of Chemical and Metallurgical Engineering, University of Witwatersrand, Private Bag 3, Johannesburg 2050, South Africa. [2]Department of Mining, Materials and Petroleum Engineering, Jomo Kenyatta University of Agriculture & Technology, Nairobi, Kenya. [3]Department of Mechanical Engineering Science, University of Johannesburg, Johannesburg, South Africa. [4]Dedan Kimathi University of Technology, Private Bag, Nyeri, Kenya. [5]Department of Metallurgical and Materials Engineering, Federal University of Technology, P.M.B 704, Akure, Nigeria.

SN Applied Sciences (2019) 1:1044 | https://doi.org/10.1007/s42452-019-1087-y

Received: 14 May 2019 / Accepted: 13 August 2019 / Published online: 16 August 2019

the production cost and time [15]. Researchers have used FEM simulation codes to study various aspects of metal forming processes for the prediction of deformation loads and metal flow behavior [11–13]. In this study, Deform® 3D FEM simulation code has been used for the simulation of real industrial upsetting (forging) process of X20CrMoV121 steel to show the effect of the deformation temperature on plastic deformation behavior. The X20CrMoV121 steel is chosen because of its extensive industrial application and there are limited publications on FEM analyses of this material.

## 2 The principle of the finite element method

The detailed description of FEM formulation for metal working process used in DEFORM® 3D software for rigid-viscoplasticity is not covered herein. However, the general equation based on the variational principle that can be used to solve rigid-viscoplastic field equations is as given in Eq. 1:

$$\delta\varphi = \int_v \sigma_i \delta\dot{\varepsilon}_i dv + \int_v K\dot{\varepsilon}_v \delta\dot{\varepsilon}_v dv - \int_{SF} F_i \delta u_i ds = 0 \quad (1)$$

In Eq. 1, $\sigma_i$ and $\varepsilon_i$ are the effective stress and effective strain respectively, $u_i$ the surface velocity components, SF is the surface force, $F_i$ is the traction stress, $\dot{\varepsilon}_v$ is the volumetric strain rate and K is a large positive penalty constant. In FEM analysis, Eq. 1 is converted into a non-linear algebraic equation through a discretization procedure. The solution to the resulting simultaneous equations is determined using an iteration process [12].

In most numerical analyses, the temperature distribution is assumed to be constant during the deformation process. However, a constant temperature in the metal-working process is unattainable due to the heat generated at the plastic deformation stage. As such, the temperature distribution during the deformation process should be considered and can be obtained by solving the Fourier energy balance Eq. 2.

$$\nabla^T(K\nabla T) + \dot{q} = \rho C_p \frac{\delta T}{\delta t} \quad (2)$$

In which K is the conductivity, T is the temperature, $\dot{q}$ is the rate of heat generation during the plastic deformation stage, ρ is the density of the material under consideration, $C_p$ is the specific heat capacity and t is time. Furthermore, the friction between the anvil-workpiece interface is mainly assumed to be of shear type (μ = 0.3) in most analyses. However, the flow stress analysis has shown that friction is a function of strain and temperature [11]. The frictional shear stress ($\tau_f$) is considered in this analysis and is expressed according to Eq. (3).

$$\tau_f = -mk\left[\frac{2}{\pi}\tan^{-1}\left(\frac{\vec{v}_s}{\mu_0}\right)\right]t \quad (3)$$

where m is the frictional coefficient factor that can be obtained from the specimen geometry (0≤m≤1), $\vec{v}_s$ is the surface velocity factor of the specimen to the anvil, K is the shear local flow stress, $\mu_0$ is a constant ($\mu_0 << \vec{v}_s$) and t is the unit vector in the direction of the surface velocity vector.

## 3 Finite element method

In this study, Design of Environment for Forming (DEFORM 3D v6.1) software was used [12, 16–18]. The properties of the X20CrMoV121 steel as available in the software database were used. The FEM model for the material geometry and die assembly were drawn using the primitive modeler in the Deform® 3D module. The dimensions of the rectangular billet and die face were 80 × 80 × 150 mm and 200 × 200 x 50 mm respectively. The forging reduction was from 150 mm to 50 mm. The forging simulation process was conducted at a deformation temperature range of 800 °C to 1100 °C and at a constant strain rate of 1 $s^{-1}$. Most of the industrial hot forging processes of steel are undertaken within this temperature range. The upper and lower dies were set to be rigid bodies, with the upper die moving at a velocity of 5 mm/sec and lower die stationary. The FEM simulation conditions and the physical properties of the deformed billet are: (a) the specimen was discretized into 36,927 tetrahedron elements and 7783 nodes with a refined mesh of the whole volume of the specimen (b) the friction type between the die and the billet was assumed to be of shear type and the constant friction was taken to be 0.3. In bulk deformation process, shear type friction is mostly assumed due to the shear deformation behavior of the material and the typical friction values range between 0.2 and 0.9. Therefore a friction coefficient value of 0.3 was taken to represent graphite lubrication, which is usually used between the die and specimen. (c) for deformation analysis, the elastic region was neglected since the forging process normally involves large deformations at high temperatures (d) the simulation was undertaken at room temperature of 20 °C and an isothermal mode of simulation was adopted. The die temperature was taken as 250 °C (e) the conventional coefficient to the environment was taken as 0.02 N/(s mm °C) and finally (f) the heat transfer coefficient between the platen and the deformed cylinder was taken as 5 W/($m^2$ K) (g) for simulation control, Lagrangian incremental simulation type with direct method for

iteration process, global remeshing, relative interference depth type and conjugate-gradient solver were chosen.

## 4 Results and discussions

### 4.1 Effect of forging temperature on forging load

A plot of forging load versus stroke at different temperatures and constant strain rate of 1 $s^{-1}$ is shown in Fig. 1. As shown, as the temperature increases, there is a decrease in the forging load. The decrease in forging load can be attributed to the fact that high temperature enhances dislocation motion and softening of metals such that the energy required for deformation is lower. 3. The relationship can also be attributed to generation of dislocation density leading to work hardening as the dominant deformation mechanism. These results indicate the dependency of forging load on the temperature [19, 20]. The forging load increases rapidly during the initial stages of the deformation process, suggesting that work hardening is the dominant deformation mechanism in this stage [19, 21–27]. Thereafter, the forging load increases gradually until a stroke of about 70 mm. This steady increase in deformation load might suggest the existence of softening mechanisms occurring. However, there was still resistance to metal flow due to the continuous increase of dislocation density [19], hence work hardening rate was dominant than the dynamic softening mechanism. As the deformation continues up to a stroke of about 70 mm a sudden increase in forging load was observed and more pronounced at lower forging temperature (800 °C and 900 °C) as shown in Fig. 1. This abrupt increase in forging load at higher deformation levels was attributed to the interfacial friction between the workpiece and the die [13].

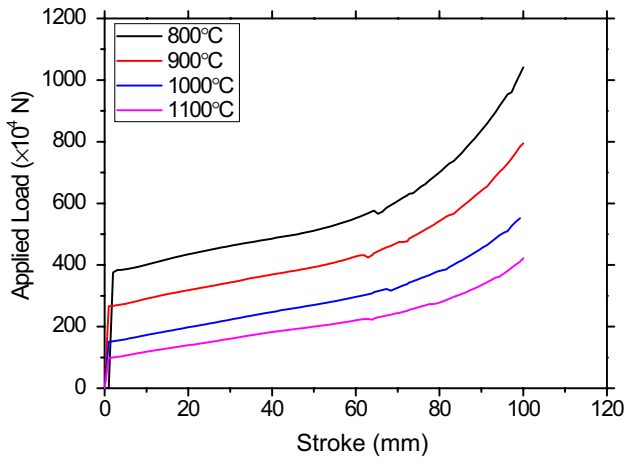


**Fig. 1** The forging load-stroke flow curves at different forging temperatures and constant strain rate of 1 $s^{-1}$

During hot deformation process the friction coefficient is not constant but vary as the lateral surface of the workpiece contacts the die at higher strain [25], hence increasing the flow stress [13]. Li et al [25] pointed out that at higher deformation levels the friction coefficient can be as higher as 1 due to static friction thus leads to an abnormal increase of forging loads. Therefore, the load-stroke flow curves correction is needed to predict the actual forging loads required in any hot forging process.

### 4.2 Effect of forging temperature on the deformation parameters

The forging temperature greatly influences the metal flow behavior during the hot deformation process. The strain, stress and particle flow velocity as influenced by the forging temperature at a constant strain rate of 1 $s^{-1}$ to the deformation degree of 67% (height reduction) is as shown in Figs. 2, 3 and 4. It was observed that the highest effective strain is located at the center of the billet with the outer layers recording lower strain values as shown in Fig. 2, suggesting an inhomogeneous deformation process [28]. The effective stress distribution is also inhomogeneous in the deformed billet (Fig. 3), the highest effective stress was observed at regions with small strains [29]. The effective stress and strain decrease with the increase in temperature during forging as observed in Figs. 2 and 3. As the deformation (forging) temperature increases, the flow stress decreases at a given strain rate and vice versa. At a constant deformation temperature and strain rate, the flow stress increases up to a peak stress at peak strain. After peak strain the flow stress attains steady state flow stress and the strain increases for a material exhibiting dynamic recovery softening mechanism. However, for dynamic recrystallization, after peak strain the flow stress drops as the strain increases until a steady state flow stress is attained. The maximum effective stress decreases as the forging temperature increases as shown in Fig. 3, hence lower forging load is required at higher forging temperature. Moreover, the standard deviation of the effective stress and strain distribution decreases with forging temperature indicating still inhomogeneous stress and strain distribution during the whole forging process.

Under the compression loading conditions, it was observed that the material particles tend to move to the nearest material surface boundary as shown in Fig. 4, as reported also in the literature [27]. The total velocity of the particle depends on its position in the material being deformed. The velocity of the particle at the edge of the billet was observed to be higher followed by the particles at the intermediate region while the particles at the bottom of the billet had the lowest total velocity (Fig. 4). The standard deviation decreases with an increase in

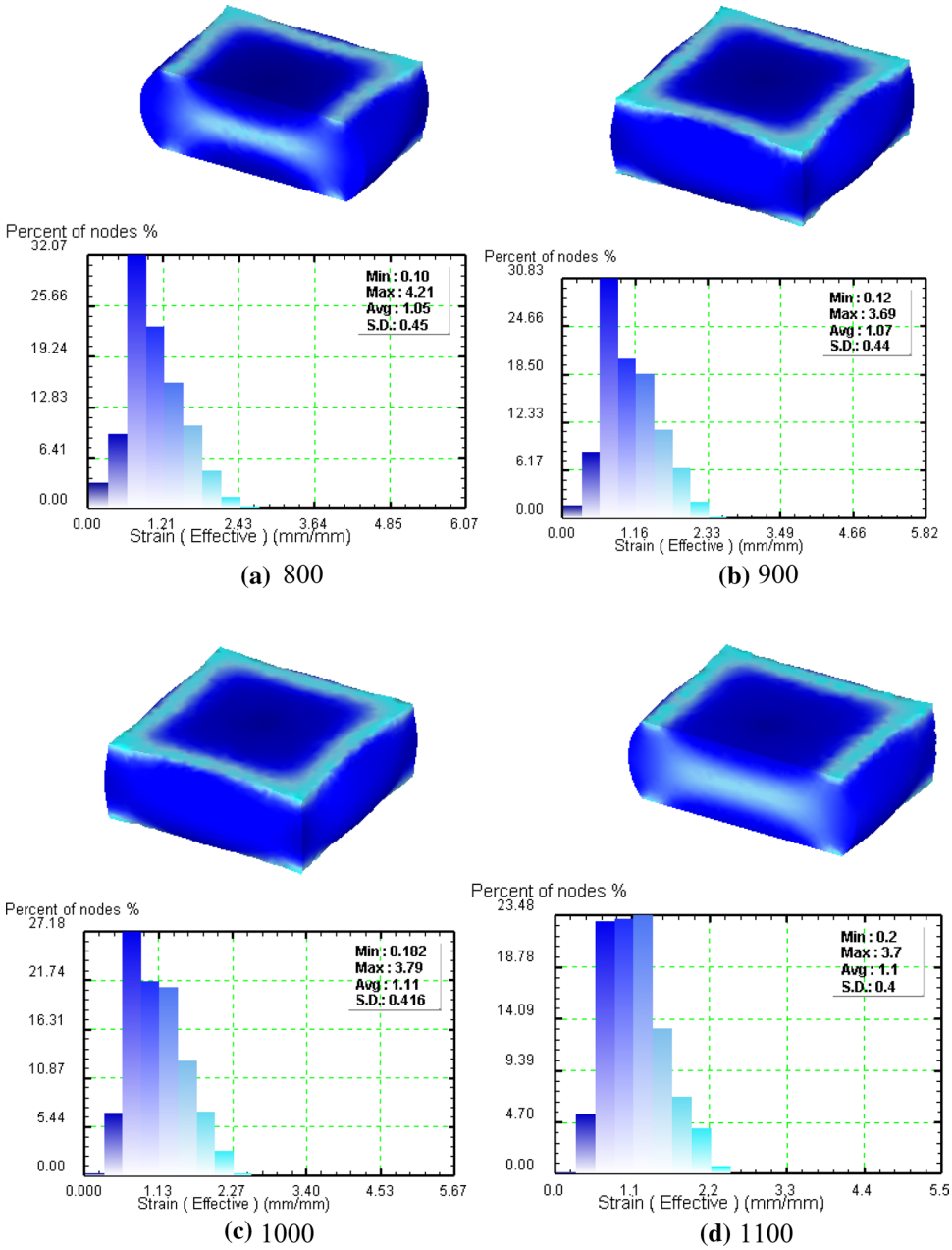


**Fig. 2** The effect of temperature on strain distribution in the deformed billet at a strain rate of 1 $s^{-1}$ and deformation degree of 66% at: **a** 800 °C, **b** 900 °C, **c** 1000 °C, **d** 1100 °C

temperature from 800 °C to 1000 °C implying that the deformation process is inhomogeneous (Fig. 4).

### 4.3 The effective strain and stress distribution

The FEM simulation time for the whole forging process was 19.6 s. The representation of the strain distribution on the deformed billet is as shown in Fig. 5. The deformation was not uniformly distributed across the billet, with the edge and side angles experiencing higher deformations as seen in Fig. 5(a). As mentioned earlier, the heterogeneous deformation exhibited during the hot forging process is attributed to interfacial frictional forces [28, 29]. The existence of frictional forces leads to three deformation zones as shown in Fig. 5(b). The three zones are categorized as dead zone (B) which is adjacent to the die surface and undergoes the least deformation due to frictional forces, moderate zone (A) and intense shear zone (C) [30].

The change in strain and stress distribution during the entire forging process can be illustrated by taking four points on the deformed billet as shown in Fig. 5(a). The strain distribution of the 4-points was presented as given in Fig. 6 at all forging temperatures. It was observed that point 1 showed a common behaviour of continuous strain increase for all forging temperatures. The higher strain was attributed to the restricted deformation by

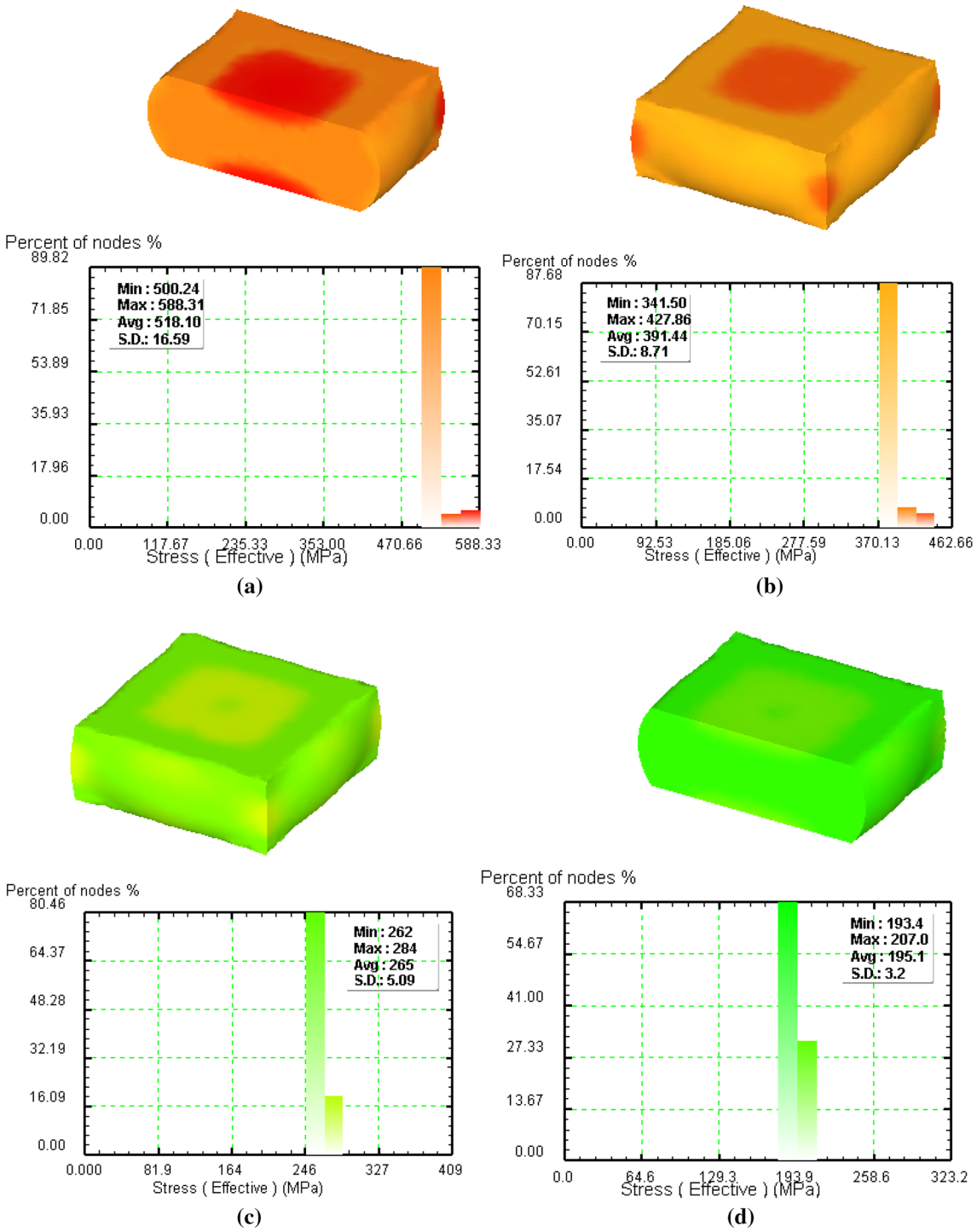


**Fig. 3** The effect of forging temperature on the stress distribution in the deformed billet at a strain rate of 1 $s^{-1}$ and deformation degree of 66% at: **a** 800 °C, **b** 900 °C, **c**1000 °C, **d** 1100 °C

the billet edge angle. Points 2 and 3, exhibited similar strain curves but with different strain values. Point 2 experienced the least strain due to frictional stress acting towards the centre of the billet hence preventing lateral metal flow [31–33]. The edge surface provides resistance to the metal flow, point 3 also experiences lower strain than point 4 but higher than point 2. On point 4, the higher strain was recorded leading to severe plastic deformation, which in turn may enhance recrystallization hence refinement of grain structures.

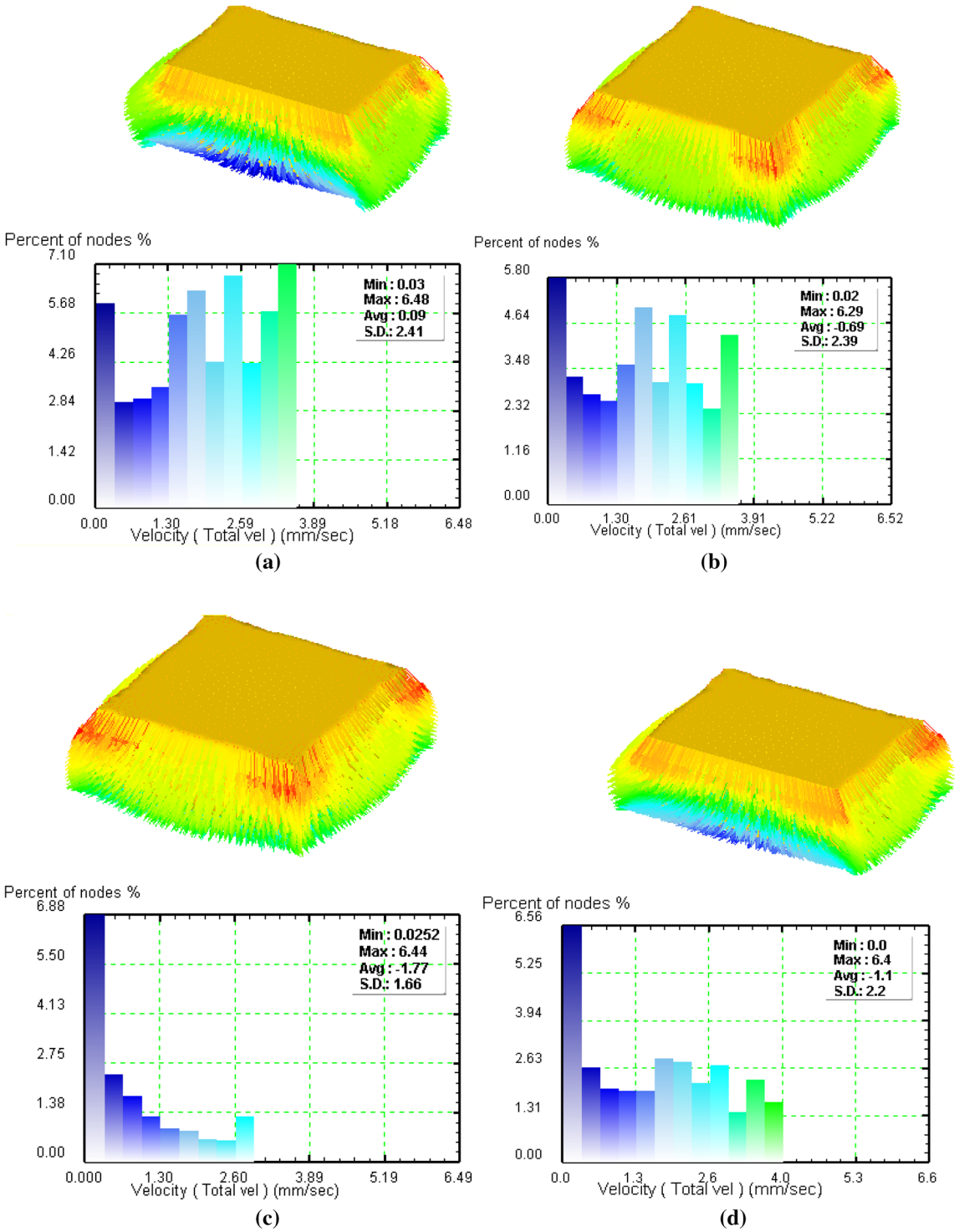


**Fig. 4** The effect of forging temperature on the particle flow velocity in the deformed billet at a strain rate of 1 $s^{-1}$ and deformation degree of 66% at: **a** 800 °C, **b** 900 °C, **c** 1000 °C, **d** 1100 °C

The stress distribution of the 4-points for the simulated conditions is shown in Fig. 7. All the points exhibited a rapid increase in stress at the beginning of the deformation process. Point 1, 3 and 4, recorded the highest effective stress at the intermediate stage of deformation. This can be attributed to the edge angle and side surface which restricted the plastic deformation leading to high stresses and strain at all forging conditions. For point 2, it

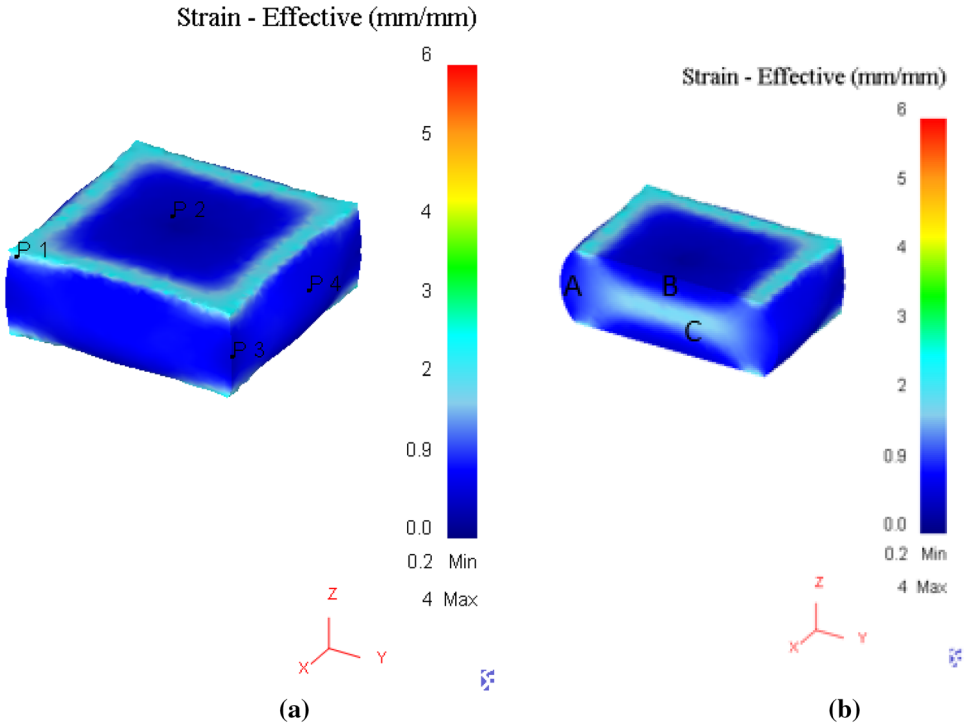


**Fig. 5** Strain distribution of the deformed billet **a** strain changes in four points: P1, P2, P3, P4, **b** deformation zones: A, B, C

showed a sharp drop in the stress curve in the intermediate region at forging temperature of 800 °C up to 12.6 s. This fluctuation in stress at this region might be associated with the restriction of metal flow or change in deformation temperature [15]. However, after 12.6 s the stress at point 2 increased gradually until the end of the forging process. For other forging temperatures, a gradual increase in stress was observed which might be a result of a decrease in the deformation temperature. From this analysis, it has been shown that at the edge angle and side surface of the billet experiences high stresses and strains. In the industrial production process, the processing route of the metal components is through the casting of billets which are prone to casting defects. Then, defects at or near the casting surface might act as crack initiators when subjected to the forging process. Since it has been shown that high stress and strain occur at the edge angles and side surfaces of the billet. But, internal defects from the casting process such as pores and voids might be welded together during the forging process hence improving the quality of the final product.

### 4.4 Particle flow velocity distribution

The total velocity distribution of the four points selected on the deformed billet after the FEM forging process simulation for the three forging temperatures and the strain rate of 1 $s^{-1}$ is presented in Fig. 8. In metal forging process, the workpiece is subjected to compressive forces which exert pressure on the particles of the material. Due to high compressive forces, the particles tend to move towards the nearest free surface at different flow velocities. The flow velocity will depend on the amount of applied force and the position of the particle in the billet (Fig. 4). The particles on the outer surface and edge angle of the billet exhibited higher velocity compared to the internal particles. It has been shown that the velocity of the 4-points selected increase rapidly during the beginning of forging process up to the time of 2.0 s for all forging temperatures considered (Fig. 8). After 2.0 s of forging, point 2 maintained a constant flow velocity of 5 mm/sec for the entire process. This constant flow velocity can be attributed to the resistance to deformation due to friction forces at the workpiece and die interface. Point 1 recorded the highest flow particle velocity compared with the other points for all forging temperatures. This indicates that the particles at the corner edge of the billet in contact with the flat surface of the die experience high compressive forces and free to move. Points 3 and 4 exhibit almost similar flow velocity since they are located at half the height of the billet since likely to experience equal compression forces. In general, the total flow velocity for points 1, 3, and 4 was observed to increase with an increase in the forging temperature, hence, suggest less resistance to metal flow at high forging temperatures.

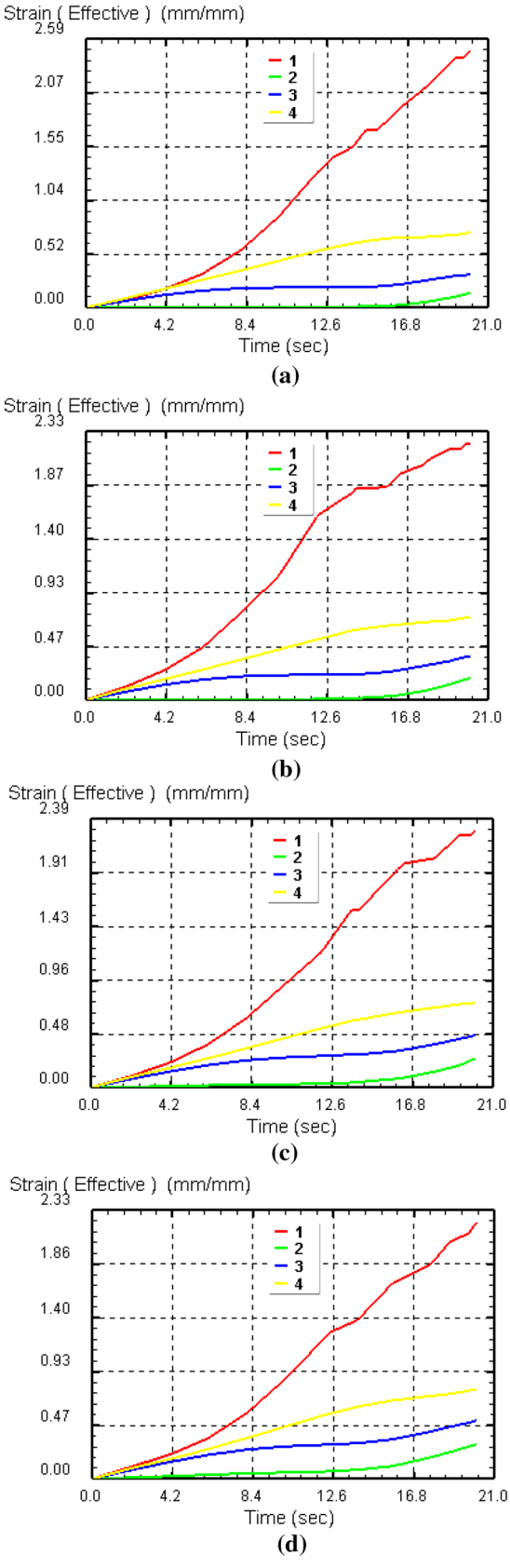


**Fig. 6** Effective strain curves for the four points on the billet **a** 800 °C, **b** 900 °C, **c** 1000 °C, **d** 1100 °C

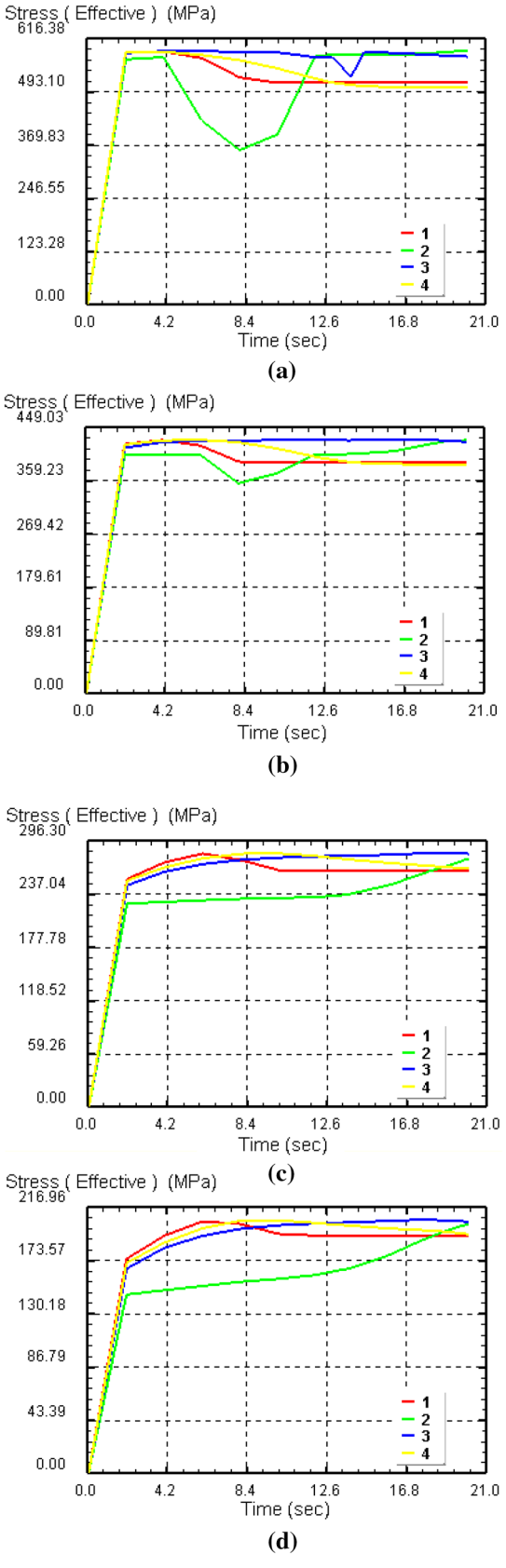


**Fig. 7** Effective stress curves for the four points on the billet **a** 800 °C, **b** 900 °C, **c**, 1000 °C **d** 1100 °C

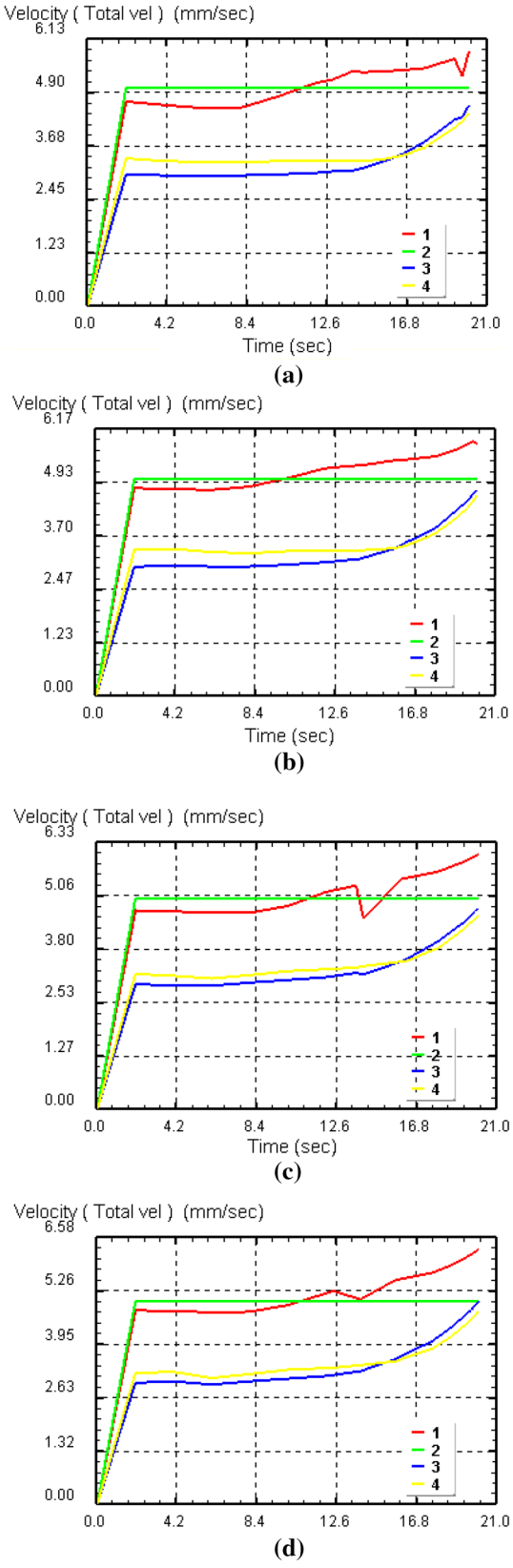


**Fig. 8** Variation of velocity (total velocity) along the deformation direction for the four points on the billet **a** 800 °C, **b** 900 °C, **c** 1000 °C, **d** 1100 °C

## 5 Conclusion

The hot forging process of the rectangular billet was analysed using Deform 3D FEM simulation code. The simulation analysis compared the stress, strain and metal particle flow velocity at a forging temperature range of 800 °C to 1100 °C for an interval of 100 °C and the strain rate of 1 $s^{-1}$. From the study, the following were the observations:

- The hot forging process results in inhomogeneous deformation of the billet with the effective strain located at the centre of the billet. The maximum effective stress occurred in regions that experienced lower strain. The variation in the standard deviation further confirmed the inhomogeneity of the forging process.
- The corner edge of the billet (point 1) had the highest strain in all the forging temperatures compared to other selected points on the deformed billet. Point 2 and 3 experienced the highest effective stress at all forging temperatures.
- The metal particle flow velocity was observed to increase with an increase in the forging temperature suggesting lower resistance to deformation process at higher forging temperature. Thus, the results agree with the real industrial forging process, hence computer simulation can provide a reliable solution for predicting the metal billet flow behaviour during the forging process.

### Compliance with ethical standards

**Conflict of interest** The authors declare that they have no conflict of interest.

## References

1. Maarefdoust M (2012) Simulation of finite volume of hot forging process of industrial gear. Int Proc Comput Sci Inf Technol 57(Icni):111–115
2. Vostrov VN, Kononov PV (2016) Finite-element simulation of flanging in the deform 3D software package. Russ Metall 2016(5):461–466
3. Beddoes J, Bibby MJ (1999) Principles of metal manufacturing processes. Butterworth-Heinemann, Oxford
4. Dieter G (1988) Mechanical metallurgy. McGraw Hill, New York
5. Lin YC, Chen MS, Zhong J (2008) Numerical simulation for stress/strain distribution and microstructural evolution in 42CrMo steel during hot upsetting process. Comput Mater Sci 43(4):1117–1122
6. Lin YC, Xia YC, Chen XM, Chen MS (2010) Constitutive descriptions for hot compressed 2124-T851 aluminum alloy over a

wide range of temperature and strain rate. Comput Mater Sci 50(1):227–233
7. Yang C, Lin X (2016) The forming analysis of two-stage extrusion for 1010 fastener. J Mech Eng Autom 6(3):43–50
8. Mehtonen SV, Karjalainen LP, Porter DA (2013) Materials science and engineering a hot deformation behavior and microstructure evolution of a stabilized high-Cr ferritic stainless steel. Mater Sci Eng A 571:1–12
9. Pu E, Zheng W, Xiang J, Song Z, Li J (2014) Hot deformation characteristic and processing map of superaustenitic stainless steel S32654. Mater Sci Eng A 598:174–182
10. Liu XG, Ji HP, Guo H, Jin M, Guo BF, Gao L (2013) Study on hot deformation behaviour of 316LN austenitic stainless steel based on hot processing map. Mater Sci Technol 29(1):24–29
11. Sun SL, Zhang MG, He WW (2010) Hot deformation behavior and hot processing map of P92 Steel. Adv Mater Res 97–101:290–295
12. Lin YC, Chen MS, Zhong J (2009) Effects of deformation temperatures on stress/strain distribution and microstructural evolution of deformed 42CrMo steel. Mater Des 30(3):908–913
13. Evans RW, Scharning PJ (2001) Axisymmetric compression test and hot working properties of alloys. Mater Sci Technol 17(8):995–1004
14. Oh SI, Wu WT, Tang JP, Vedhanayagam A (1991) Capabilities and applications of FEM code deform: the perspective of the developer. J Mater Process Technol 27(1–3):25–42
15. Zhang ZJ, Dai GZ, Wu SN, Dong LX, Liu LL (2009) Simulation of 42CrMo steel billet upsetting and its defects analyses during forming process based on the software DEFORM-3D. Mater Sci Eng A 499(1–2):49–52
16. Ji YH, Park JJ (2009) Development of severe plastic deformation by various asymmetric rolling processes. Mater Sci Eng A 499(1–2):14–17
17. Lee YS, Lee SU, Van Tyne CJ, Joo BD, Moon YH (2011) Internal void closure during the forging of large cast ingots using a simulation approach. J Mater Process Technol 211(6):1136–1145
18. Na YS, Yeom JT, Park NK, Lee JY (2003) Simulation of microstructures for Alloy 718 blade forging using 3D FEM simulator. J Mater Process Technol 141(3):337–342
19. Zhu L, He J, Zhang Y (2018) A two-stage constitutive model of X12CrMoWVNbN10-1-1 steel during elevated temperature. Mater Res Express 5:026505
20. Francis JA, Mazur W, Bhadeshia HKDH (2006) Review type IV cracking in ferritic power plant steels. Mater Sci Technol 22(12):1387–1395
21. Skobir DA, Vodopivec F, Kosec L, Jenko M, Vojvodič-Tuma J (2004) Influence of precipitates size and distribution on room temperature mechanical properties and accelerated creep of X20CrMoV121. Steel Res Int 75(3):196–203
22. Ohgami M, Naoi H, Kinbara S, Mimura H, Ikemoto T, Fujita T (1997) Development of 9CrW tube, pipe and forging for ultra supercritical power plant boilers. Nippon Steel Tech Rep 72:59–64
23. Park JJ (1984) Three-dimensional finite element analysis of block compression. Int J Mech Sci 26(3):165–176
24. Osakada K, Nakano J, Mori K (1982) Finite element method for rigid-plastic analysis of metal forming: formulation for finite deformation. Int J Mech Sci 24(8):459–468
25. Li YP, Onodera E, Matsumoto H, Chiba A (2009) Correcting the stress-strain curve in hot compression process to high strain level. Metall Mater Trans A Phys Metall Mater Sci 40(4):982–990
26. Equbal MI, Talukdar P, Kumar V, Ohdar RK (2014) Deformation behavior of micro-alloyed steel by using thermo mechanical simulator and finite element method. Procedia Mater Sci 6(Icmpc):674–681
27. Ahmad A, Lajis MA, Shamsudin S, Yusuf NK (2018) Conjectured the behaviour of a recycled metal matrix composite (MMC-AlR) developed through hot press forging by means of 3D FEM simulation. Materials (Basel) 11(6):958
28. Kumar SD, Mandal A, Chakraborty M (2015) On the age hardening behavior of thixoformed A356-5TiB2 in-situ composite. Mater Sci Eng A 636:254–262
29. Rahul MR, Samal S, Venugopal S, Phanikumar G (2018) Experimental and finite element simulation studies on hot deformation behaviour of AlCoCrFeNi2.1 eutectic high entropy alloy. J Alloys Compd 749:1115–1127
30. Kingkam W, Li N, Zhang HX, Zhao CZ (2017) Hot deformation behavior of high strength low alloy steel by thermo mechanical simulator and finite element method. IOP Conf Ser Mater Sci Eng 205(1):012001
31. Kajtoch J (2007) Strain in the upsetting process. Metall Foundry Eng 33(1):1–11
32. Kumar SD, Karthik D, Mandal A, Kumar JSRP (2017) Optimization of Thixoforging process parameters of A356 alloy using Taguchi's experimental design and DEFORM Simulation. Mater Today Proc 4:9987–9991
33. Kumar SD, Mandal A, Chakraborty M (2015) Effect of thixoforming on the microstructure and tensile properties of A356 alloy and A356-5$TiB_2$ in-situ composite. Trans Indian Inst Met 68(2):123–130